Applied Catalysis B: Environmental 314 (2022) 121456

Contents lists available at ScienceDirect

Applied Catalysis B: Environmental

journal homepage: www.elsevier.com/locate/apcatb

Efficient and continuous chemical conversion in a thin membrane comprising three-dimensional network trapping Ag nanoparticles

Yuhua Mao, Hao Zhang, Saad Ahmed, Shanshan Li, Shouhao Zhang, Jianli Wang *

State Key Laboratory Breeding Base of Green Chemistry-Synthesis Technology, Zhejiang Province Key Laboratory of Biofuel, Biodiesel Laboratory of China Petroleum and Chemical Industry Federation, College of Chemical Engineering, Zhejiang University of Technology, Hangzhou 310014, PR China

ARTICLE INFO

Keywords:
Hybrid microgels
Catalytic membrane
Silver nanoparticles
Heterogeneous catalysis
4-Nitrophenol

ABSTRACT

In this work, we report a novel and highly efficient catalytic membrane (PES/PNM-Ag) comprising well-dispersed silver nanoparticles (NPs). The membrane can be straightforwardly constructed via dynamic loading expansible hybrid microgels PNM-Ag into a commercially-available poly(ether sulfone) (PES) membrane with asymmetric structure. Characterization results of PNM-Ag and PES/PNM-Ag indicate that a nanoscale three-dimensional network embedded with Ag NPs was developed in membrane pores by swollen microgels. The flat-sheet membrane reactor assembled with PES/PNM-Ag can efficiently and continuously catalyze the reduction of 4-nitrophenol (apparent reaction rate constant reaching 1.12 s^{-1}) and showed good stability. The improved catalytic activity was attributed to fully accessible surface of Ag NPs as well as the unique structure of the membrane, in which the reactant was restricted to flow through immobilized catalyst. Present strategy hints to design other noble metal NPs loaded catalytic membranes for efficient conversion of nitro-aromatic pollutants.

1. Introduction

Smart polymer microgels are three-dimensional colloidal particles that exhibit abrupt size variation due to their sensitivity to the medium's temperature and pH [1,2]. This high adaptability and responsive nature have made them a topic of contemporary research. Chemical separation sensing and catalysis are only a few applications for smart polymer microgels [3–5].

Noble metal nanoparticles (NMNPs) are often employed to catalyze different reactions such as the oxidation of automobile exhaust [6,7], cross-coupling reactions [8,9] and selective hydrogenation [10,11]. NMNPs are frequently employed in catalysis owing to their atomically rich surface, high surface-to-volume ratio, as well as a distinctive electronic structure [12–14]. However, the disadvantage associated with NMNPs is their high surface energy, which causes aggregation and ultimately leads to a significant loss of activation [15,16]. To overwhelm the above-stated concerns, immobilization of NMNPs on a support material is contemplated as a promising strategy to reinforce stability and recyclability [17,18]. A polymeric system can hinder NMNPs from coalescence and lead to increased stability. Microgels not only help to maintain NMNPs stable for an extended period, but they also help to boost their catalytic activity by allowing reactants to diffuse more easily to the NMNPs surface [19–21]. Additionally, the catalytic activity of NMNPs incorporated microgels can be regulated by varying external stimuli. Microgels are regarded as microreactors for the synthesis of NMNPs, in which functional groups can well regulate the size and size distribution of NMNPs by interacting with precursor ions [22]. Different NMNPs such as Pt, Pd, Au, and Ag NPs formed in microgels networks have been frequently used for the reduction of numerous nitroaromatic compounds. On the contrary, Ag NPs are least expensive than other NMNPs while providing comparable catalytic performance. For instance, Zhang et al. disposed Ag NPs@CMG hybrids aerogels to be a porous membrane for catalyzing and simultaneous product separation [23].

The catalytic membrane reactor (CMR) is a method for process intensification that combines catalytic activity and membrane operation into a single unit [23,24]. CMR has several benefits, including a small footprint, lower equipment costs, less energy use, and higher efficiency. Additional advantages include (a) avoiding the requirement to disperse and separate the catalyst from the reaction mixture, (b) improving the transformation of thermodynamically restricted reactions through in-situ product elimination (c) intermediate products removal, improving selectivity for subsequent reactions (d) long term use and uninterrupted catalysis beyond the need to recycle the catalyst [25,26].

* Corresponding author.
E-mail address: wangjl@zjut.edu.cn (J. Wang).

https://doi.org/10.1016/j.apcatb.2022.121456
Received 13 January 2022; Received in revised form 24 April 2022; Accepted 25 April 2022
Available online 28 April 2022

Recently, catalytic non-permselective membrane reactors (CNMRs) with no separating characteristics have attracted researchers [25,27,28]. They have been effectively used as microstructured reactors to offer a reaction space by a short and regulated residence time and higher catalytic activity. A non-separating and micro porous catalytic membrane is used for flow-through reactions in dead-end mode. The forced flow of reactants through the membrane increases the interaction among reactants and immobilized catalysts, resulting in high catalytic activity and low mass transport resistances [25]. The inverse filtration of a polyvinylidene fluoride (PVDF) membrane with gold (Au) assembled NPs achieved outstanding stability for the catalytic reduction of 4-NP and methylene blue (MB), with conversion rates of 75% and 78%, correspondingly [27]. Similarly, CNMR based on polyether sulfone (PES) showed improved catalytic activity for cellulose [28]. Furthermore, the open-pore channels of catalytic membranes permit substances to enter/exit via forced convection while also shortening the diffusion distance [29]. The catalytic membrane is regarded as a process intensifier and a continuous flow reactor [30,31]. However, NMNPs in the reported catalytic membranes prepared by blending method were inevitably covered by the membrane matrix, resulting in a reduction of available catalytic active sites. For the in-situ reduction method, a complicated functionalization of the pore surface of the membranes was required, resulting in uncertain loading of NMNPs.

Herein, a novel catalytic membrane with a 3D network structure was prepared by the dynamic filtration method, where thermo- & pH- dual-responsive Ag NPs microgels in proper size were introduced into a piece of highly asymmetric microporous membrane (Fig. 1). The hybrid microgel can expand and form a distinct network in membrane pores. Moreover, the steadiness of the 3D network in the pores was confirmed by a filtration test. In the presence of PES/PNM-Ag, the catalytic conversion of 4-NP into 4-aminophenol (4-AP) was observed. The catalytic performance of the membrane to convert 4-NP in an aqueous medium under numerous conditions was also analysed.

2. Experimental section

2.1. Materials

N-isopropylacrylamide (NIPAM, 99%), methyl acrylic acid (MAA, 99%), N, N′-methylenebis (acrylamide) (BisAM, 99%), potassium persulfate (KPS, ≥99%) and sodium dodecyl sulfate (SDS, ≥99%) were purchased from Aladdin Co. China Ltd. Silver nitrate ($AgNO_3$, ≥99%), chloroplatinic acid hexahydrate (>99.9%), sodium borohydride ($NaBH_4$, 98%) and 4-nitrophenol (4-NP, 99%) were purchased from Energy Chemical Co. China Ltd. NIPAM was purified by recrystallization, and MAA was purified by an inhibitor remover column. Other chemicals were used as received. Poly(ether sulfone) (PES) membrane (Catalog Number: HPWP04700) with a highly asymmetric textile structure was purchased from Merck Millipore. Deionized (DI) water was produced by a Aquelix5 apparatus (Millipore, America).

2.2. Synthesis of P(NIPAM-co-MAA) microgels

The microgels were synthesized according to literature by following procedure [32]. Firstly, at an ambient temperature, NIPAM (1.36 g), MAA (0.69 g), crosslinker BisAM (0.15 g) and SDS (0.01 g) were dissolved in DI water (300 mL) with stirring in a 500 mL glass reactor under N_2 atmosphere. The temperature of the reactor was increased to 70 °C, then 0.05 g KPS in 2 mL aqueous solution was injected in for initiating polymerization for 4 hrs. After that, the P(NIPAM-co-MAA) microgels were collected by a centrifugation protocol and subsequently lyophilized at −49 °C.

2.3. Synthesis of P(NIPAM-co-MAA)-Ag hybrid microgels

To prepare P(NIPAM-co-MAA)-Ag hybrid microgels, a reduction strategy was applied to make sure the tiny metal particles were uniformly dispersed in the gel. 150 mg of dry P(NIPAM-co-MAA) microgels was re-dispersed and sufficiently swollen in 250 mL of DI water at 20 °C. Then aqueous $AgNO_3$ (75 mL, 1.0 mM) was purged. After 2 h of homogenization, $NaBH_4$ aqueous solution (40 mL, 0.25 M) was added dropwise in a half hour. 4 h later, a similar protocol was used to obtain dry hybrid microgels.

2.4. Preparation of the catalytic membrane

The Ag NPs loaded microgel containing catalytic membrane was prepared by employing dynamic filtration strategy proposed by Wessling's group [33]. The suspension of a certain amount of P (NIPAM-co-MAA)-Ag hybrid microgels in water (pH=3) was dead-end filtered through a piece of asymmetric PES membrane under a vacuum (−0.09 MPa) at 30 °C. After that, the membrane was washed with a large amount of water and naturally dried.

2.5. Characterization

The hydrodynamic diameter and its distribution of hybrid microgels were measured by Dynamic Light Scattering (DLS, Zetasizer Nano ZS90, Malvern, UK).

Morphology of the hybrid microgels was visualized by using a transmission electron microscopy (TEM, Titan-G2 80–200 chemiSTEM FEI) operating at 80 KV. The elemental mapping and line scanning was charactered by a 300 kV/FEG transmission electron microscope (Tecnai G2 F30 S-Twin, Philips-FEI, Holland) equipped with an energy dispersive X-ray spectrometer (EDS) analyzer. One drop of hybrid microgel dispersion was casted on a carbon copper grid for charactering the

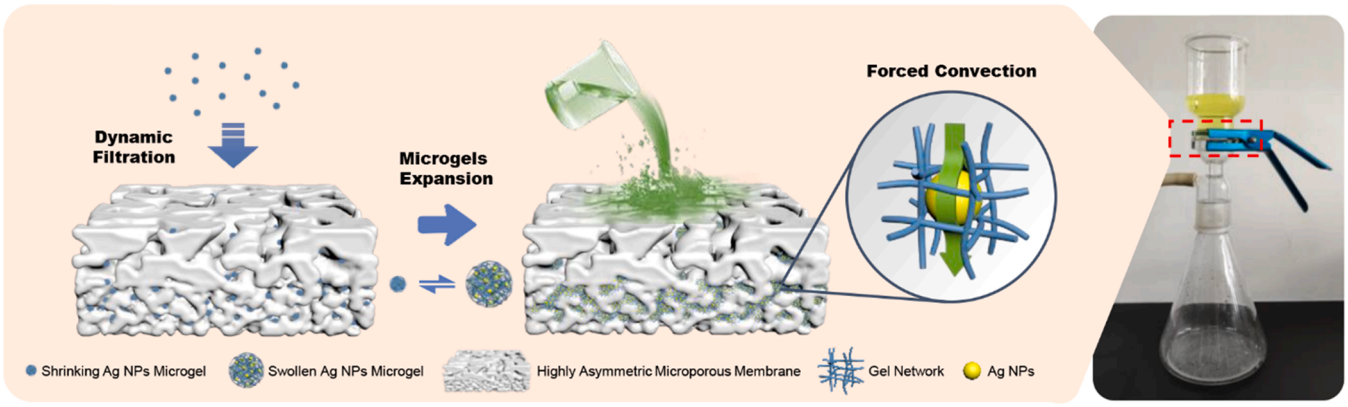

Fig. 1. Schematic illustration of the preparation and the microstructure of the catalytic membrane.

morphology and elemental distribution.

Fourier Transform Infrared spectroscopy of the hybrid microgels was recorded at room temperature in transmittance mode ranging from 400 to 4000 cm^{-1} using Fourier Transform Infrared Spectrometer (Nicolet IS10, Thermo Fisher Scientific, America) (Fig. S1).

The thermal gravimetric analysis of the hybrid micorgels was performed from 30 to 800 °C with a heating rate of 10 °C/min under N_2 atmosphere using TG 209 F3 Tarsus, Netzsch, Germany (Fig. S2).

Pore size of the nascent membrane was determined by a membrane pore size analyser (BSD-PB, BSD Instrument, China) (Fig. S3).

The morphologies of membranes were examined by a scanning electron microscope (SEM, S-4700, Hitachi, Japan). Meanwhile, the elemental composition was analyzed by equipped EDS analyzer (Fig. S4).

Ag content in the catalytic membrane was determined with an inductively coupled plasma mass spectrometer (ICP-MS, Elan DRC-e, PerkinElmer, America). For this purpose, the membrane sample was dissolved in a HNO_3/HCl solution.

UV–Visible analysis was performed by a UV–visible Spectrophotometer (Cary 60, Aglient, America).

2.6. Stimuli-responsive water flux

Dead-end filtration equipment was applied to determine the water flux of hybrid microgels modified membrane at room temperature. Before testing, every piece of the sample was pre-pressurized for 30 min at a vacuum (−0.09 MPa). The flux of aqueous solution (pH=3 or 11) was measured alternatively at −0.09 MPa. The water flux was calculated by Eq. (1).

$$J = \frac{V}{A \times t} \tag{1}$$

where J (L m^{-2} h^{-1}) is the water flux, V (L) is the volume of permeated water, A (m^2) is the membrane area (12.56 cm^2), and t (h) is the penetration time.

2.7. Catalytic performance of membrane

The conversion of 4-NP determines the performance of the PES/PNM-Ag membrane. After being pre-pressurized for 30 min at a vacuum pressure of −0.09 MPa, a mixed solution (pH=11, adjusted by NaOH) containing 4-NP (30 mg/L) and $NaBH_4$ (6 g/L) was passed through the membrane (12.56 cm^2) by dead-end filtration at 20 °C (Fig. 1). Since the concentration of the 4-NP solution is proportional to its absorbance at 400 nm, a standard curve was established (Fig. S5). The variation of 4-NP concentration was detected by UV–Vis spectroscopy.

2.8. Stability of catalytic membrane

A continuous-flow reaction system (Fig. S6) was assembled to determine the stability of the catalytic membrane. To prevent reactants from reacting during storage, aqueous solution of 4-NP (60 mg/L) and $NaBH_4$ (12 g/L) were adjusted to pH= 11 by NaOH and stored separately. The two solutions were mixed in a static mixer and then passed through the membrane reactor with a controlled flow rate (216 L m^{-2} h^{-1} (LMH)) by a peristaltic pump. It was operated continuously for 7 hrs. at 20 °C. The 4-NP concentration in the filtrate was detected by UV–Vis spectroscopy at regular intervals.

To demonstrate the storage stability, catalytic membranes after dry storage for 3 months and 6 months were moistened with deionized water and placed into the membrane reactor. After being pre-pressurized for 30 min, the same method was employed to determine the conversion rate of 4-NP under the flow rate of 216 LMH.

3. Results and discussion

3.1. Characterization of P(NIPAM-co-MAA)-Ag hybrid microgels

The free radical precipitation polymerization process was used to create P(NIPAM-co-MAA) microgels. This approach is deemed superior because it allows for narrow size distribution of P(NIPAM-co-MAA) microgel particles [32,34]. For in situ method, positively charged silver ions were attracted by negatively charged carboxylic groups and these anionic groups function as ligands to bind silver ion inside the microgels network. Furthermore, the charge transfer efficacy improves as the size of Ag NPs decreases.

DLS measurement was utilized to measure changes in the hybrid microgels diameter (Fig. 2d). Under acidic conditions at 60 °C, pH= 3, The P(NIPAM-co-MAA)-Ag microgels has Z-average diameter (Dz) of 230 nm, while at 20 °C, pH= 11 Dz increases to 880 nm. Moreover, 56 times higher volume expansion of the hybrid microgel was due to the individual microgel swelling. The morphology and size distribution of Ag nanoparticles incorporated into P(NIPAM-co-MAA)-Ag microgels were evaluated using TEM (Fig. 2a, b). In the TEM images, the P(NIPAM-co-MAA)-Ag microgels particles appear spherical. The presence of dark spots indicates that Ag NPs were loaded uniformly into each microgel particle, with an average diameter of about 7.8 nm. The majority of Ag NPs were discovered inside the microgel particles, indicating a significant donor-acceptor interaction between carboxylic acid groups (-COOH) and Ag nanoparticles. Elemental mapping images show homogeneous distribution of Ag signal in the whole microgel (Fig. 2c). Meanwhile, line scanning showed a broad peak for C corresponding to the microgel profile, while multiple peaks for Ag were uniformly distributed over this range (Fig. 2e). The two results further confirmed that Ag NPs are uniformly distributed inside the microgel but not only on the surface.

The mesh size (ξ) of swollen gel network (20 °C, pH=11) was evaluated using the Canal-Peppas equation (Eq. (2)) [35]. The average mesh size of swollen microgel was about 6 nm. Molecules having a diameter less than the mesh size can pass if their trajectory aligns to the free volume [35]. The diameter of Ag NPs loaded in the microgels was an average of 7.8 nm, indicating that the gel network can act as a physical barrier to avoid accumulation and loss. The electrostatic and coordination interactions between functional groups in microgels can also stabilize Ag NPs [22].

$$\xi = \varphi_s^{-\frac{1}{3}} \left(l^2 C_n n \right)^{\frac{1}{2}} \tag{2}$$

where φ_s is the polymer volume fraction in the swollen equilibrium state, l is the polymeric carbon-carbon bond length (l=0.154 nm), and C_n is the polymer-specific characteristic ratio for a chain of n repeating units.

3.2. Characterization of the catalytic membrane

The Ag NPs loaded microgels is utilized to modify commercially available membrane via dynamic filtration. Microgel dispersion (10 mg/L, 30 °C, pH=3) was directly filtered through a highly asymmetric microporous membrane. At a constant vacuum pressure of −0.09 MPa, microgels were introduced directly into the commercially available microfiltration membranes and retained within membrane during the filtration. The weight of the modified PES/PNM-Ag membrane was increased by 7.9 wt%. The catalytic membrane contains 3.06 mg of Ag per gram, as determined by an inductively coupled plasma mass spectrometer (ICP-MS).

The morphology of the nascent membrane and catalytic membrane PES/PNM-Ag is shown in Fig. 3. It was observed that the nascent membrane was highly asymmetric, with a pore size of 5–20 μm on the top surface and 0.45 μm in the active layer. The diameter of shrinking microgels (360 nm) is significantly smaller than the pore size on the

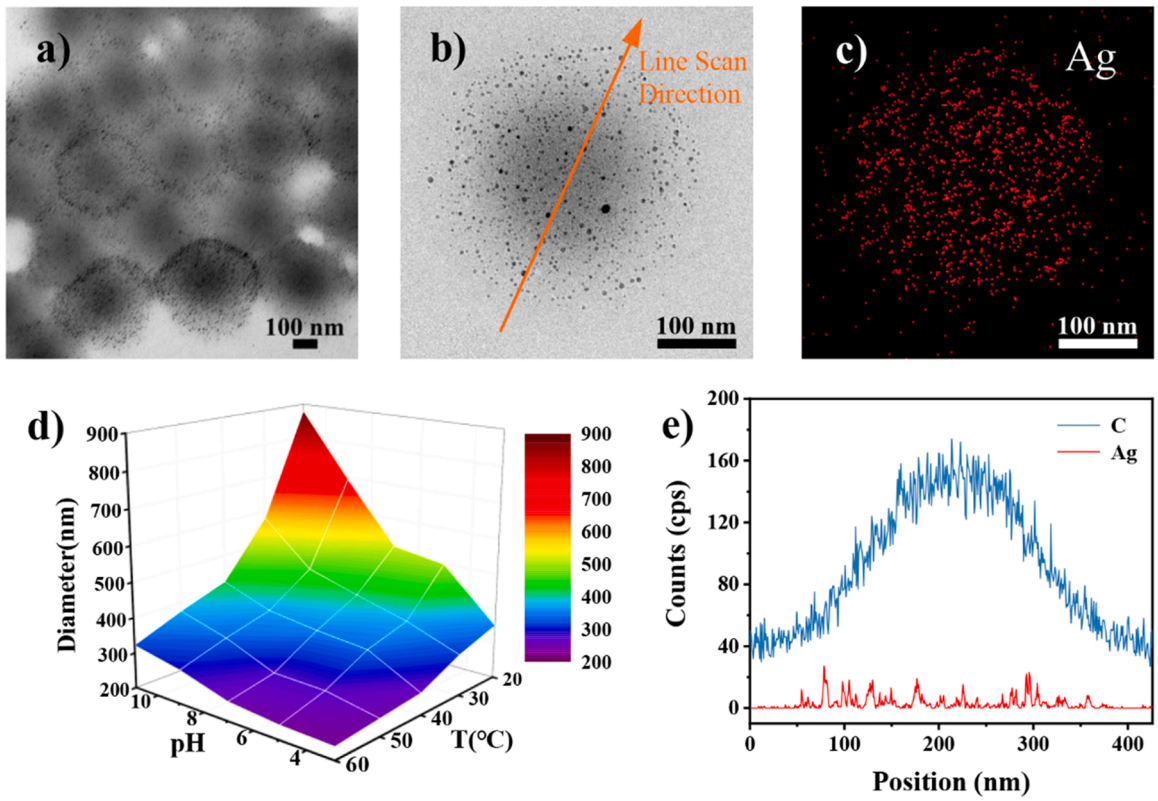

Fig. 2. (a, b) TEM images of P(NIPAM-co-MAA)-Ag. (c) Ag elemental mapping image of P(NIPAM-co-MAA)-Ag. (d) Thermo- and pH-dependent hydrodynamic diameters of P (NIPAM-co-MAA)-Ag measured by DLS. (e) EDS line scan result of P(NIPAM-co-MAA)-Ag.

upper surface of the membrane but close to the pore size in the pore throats. As a result, only a small amount of microgels were found to be adsorbed on the upper surface of the catalytic membrane. A substantial number of microgels were introduced into the membrane and retained in the active layer by size exclusion and/or adsorption during filtration. The diameter of dried microgels was about 200 nm.

Compared with the nascent membrane (33,000 LMH) at 20 °C, − 0.09 MPa, the water flux of the catalytic membrane declined dramatically (12,400 LMH at 20 °C, pH=3, −0.09 MPa). When the microgels were fully swelled (20 °C, pH=11), the water flux of the catalytic membrane dropped further to 164 LMH. The reversibility and stability of the catalytic membrane were investigated by alternatively treating with solutions at pH= 3 and 11. The reversible shift of flux was in good agreement with the diameter shift of retained microgels and remained well (Fig. 4a). In prior work, we found that a CO_2-responsive membrane prepared in the same way could reject up to 93% of bovine serum albumin (BSA), macromolecules with a hydrodynamic diameter of about 8 nm [36]. Expansion of microgels leads to the change of transportation channels. The microgels entirely blocked channels, and molecules could only pass through from the free volume of the gel network (Fig. 4b).

3.3. Catalytic performance of membrane

The conversion of 4-NP determined the catalytic performance of the PES/PNM-Ag membrane. The literature suggested that the Langmuir–Hinshelwood (L-H) adsorption model was generally used in almost all of the studies for the catalytic conversion of 4-NP [37]. At first, the 4-NP and reductant ($NaBH_4$) were adsorbed on the surface of Ag NPs and $NaBH_4$ generates active hydrogen on Ag-surface. Afterwards, the 4-NP will be reduced via electron transfer, which is dependent on (a) the rate of 4-NP adsorption on the catalyst surface; and (b) the transfer rate of electrons via the interface of catalyst surface [38]. The desorption rate of 4-AP from the catalytic surface, allowing it to be more accessible for a new cycle to begin.

According to UV results, a distinctive peak appeared at about 400 nm for the aqueous solution of 4-NP under alkaline condition. When the solution passed through the catalytic membrane, the intensity of absorbance peak at 400 nm decreased. A new characteristic peak at about 310 nm appears which depict formation of the 4-AP, indicating that 4-NP was converted (Fig. 5a). Since the absorbance at 400 nm is proportional to the concentration of 4-nitrophenol, the catalytic reduction kinetics can be investigated by tracking the change of absorbance at 400 nm. The conversion of 4-NP gradually increased as the residence time of the reactants was prolonged.

Due to the high kinetic barrier generated by the electrostatic repulsive interactions between nitro-aromatics and BH_4^- ions, the reaction was thought to proceed in the presence of catalysts [39]. Moreover, Ag NPs act as an electron relay in this reaction, accepting electrons from borohydride and donating them to 4-NP. Since the amount of sodium borohydride in the solution is excessive, the reaction is considered as pseudo-first-order and can be described by Eq. (3) [37]:

$$\ln(1-\eta) = -k_{app}\tau \tag{3}$$

Here k_{app} is the apparent rate constant of the reaction (s^{-1}), and η is the conversion rate of 4-NP. The residence time (τ, s) of the solution in membrane pores was defined as the ratio of the volume of pores to the volumetric flow rate of solution, and was calculated by Eq. (4):

$$\tau = \pi r^2 L\varepsilon / Q_v \tag{4}$$

where r, L, ε, and Q_v are the membrane radius (cm), membrane thickness (cm), membrane porosity (%), and flow rate ($mL{\cdot}s^{-1}$), respectively. The apparent rate constant of the reaction catalyzed by the catalytic membrane is 1.12 s^{-1} as shown in Fig. 5b.

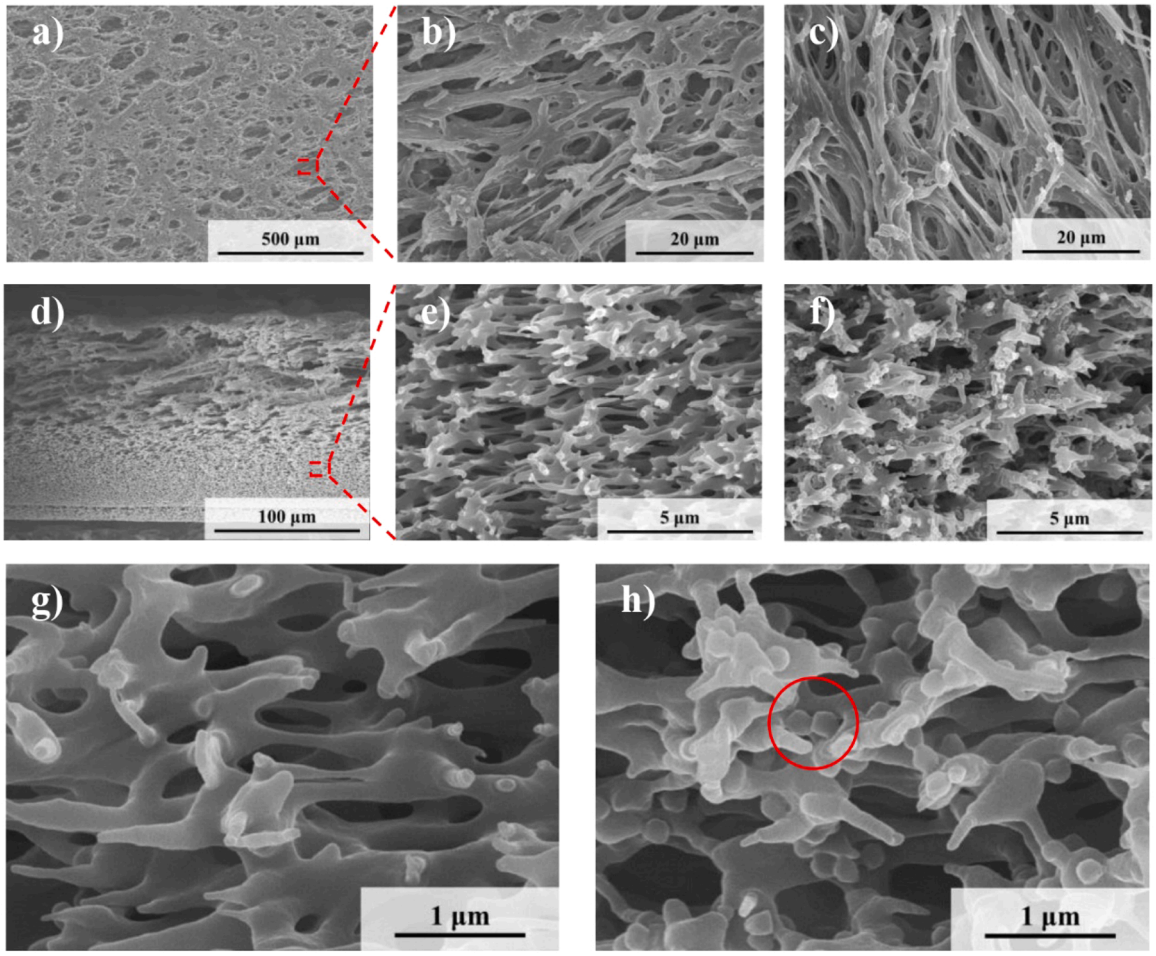

Fig. 3. (a, b) The top surface morphology of the nascent membrane and (c) the PES/PNM-Ag catalytic membrane. (d, e, g) The cross-section morphology of the nascent membrane and (f, h) the PES/PNM-Ag catalytic membrane.

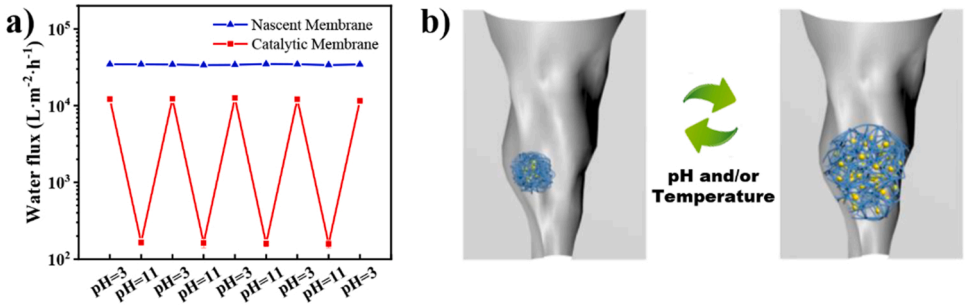

Fig. 4. (a) Water flux of the PES/PNM-Ag catalytic membrane after alternative stimulation (20 °C, −0.09 MPa). (b) Schematic representation of the change of transportation channels.

3.4. Stability of catalytic membrane

A continuous operation investigated the stability of the catalytic membrane at constant flux. It is an outstanding phenomenon, as shown in Fig. 6, that the conversion of 4-NP and the transmembrane pressure of the catalytic membrane both rose synchronously during the first 30 min of pre-pressurizing. Microgels deformed and packed densely in the pore throats under pressure. As a result, channelings were restrained and the free volume of the gel network became the only reactant pathway, leading to higher resistance and improved catalytic activity. The phenomenon is consistent with the proposed mechanism outlined above. The conversion rate and transmembrane pressure remained consistent, depicting that the microgels in the pores and the Ag NPs in the gel network were efficiently preserved. Since the diameter of swollen microgels expanded to become greater than the pore size, microgels were retained in the pores by size exclusion. The physical barriers as well as electrostatic and coordination interactions hindered Ag NPs aggregation and/or escape in the gel network.

Moreover, catalytic performance of the membranes after dry storage for 3 months and 6 months was charactered. The results show that the conversion rates of 4-NP in the reaction solutions passing through the two catalytic membranes are 82.68% and 81.00% under the condition of residence time of about 1.64 s (Fig. 6b), respectively. The two membranes showed catalytic performance close to that of the freshly

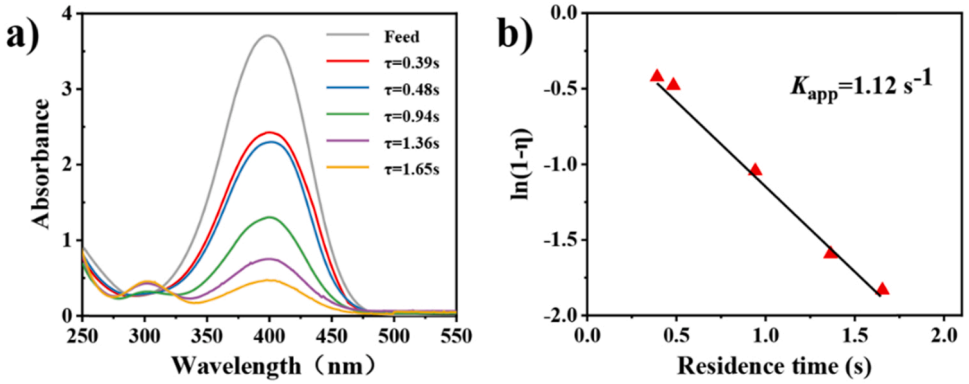

Fig. 5. (a) UV–Vis spectra of filtrate with difference residence time τ. (b) Apparent kinetic rate constant of the reduction of 4-NP catalyzed by PES/PNM-Ag membrane (20 °C; 4-NP, 30 mg/L; $NaBH_4$, 6 g/L).

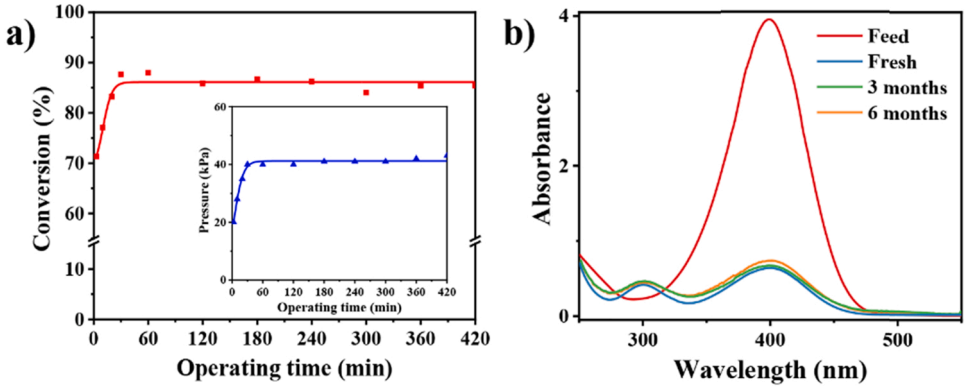

Fig. 6. (a) Conversion rate of 4-NP (20 °C; 4-NP, 30 mg/L; $NaBH_4$, 6 g/L) and transmembrane pressure at a resistance time of 1.64 s during the continuous operation. (b) UV–Vis spectra of filtrate catalyzed by freshly prepared PES/PNM-Ag membrane, recycled membrane after storage for 3 months, and 6 months.

prepared ones, indicating that the catalytic membrane remained stable after dry storage for six months.

3.5. Comparison with other reported membranes for conversion of 4-NP

Table 1 compared the k_{app} and turnover frequency (TOF) of different catalysts. All the TOF were calculated from the data when the conversion was around 85% to consider the influence of mass transfer by Eqs. (5) and (6):

$$TOF = \frac{mol_{4-NP}}{mol_{Ag} \times D \times t} \tag{5}$$

Here mol_{4-NP} is the amount of 4-NP (mol), mol_{Ag} is the amount of Ag atoms (mol), D is dispersion and t is the reaction time. The dispersion is estimated based on the diameter of the nanoparticles by Eq. (6) [45]:

$$D = 10^{21} \times \frac{6 \times M \times \rho_{site}}{d \times \rho_{metal} \times N} \tag{6}$$

M is the atomic weight (107.9 g/mol for Ag), ρ_{site} is the silver surface site density(11.5 Ag atoms/nm^2), d is particle size (nm), ρ_{metal} is the metal density (10.49 g/cm^3 for Ag) and N is the Avogadro constant.

The apparent reaction rate of the reaction catalyzed by PES/PNM-Ag is higher. Furthermore, it is being noted that catalytic activity of Ag NPs in the catalytic membrane is approximately five times higher than hybrid microgels dispersion and three times that of other catalytic membranes.

It is believed that both unique structure of the membrane and exposed active surface of immobilized Ag NPs contributed to the improvement of catalytic performance. Firstly, Ag NPs embedded in gel network are fully accessible to reactants when the microgels are sufficiently swollen [40]. When the microgels are loaded into membrane pores in this work, Ag NPs in the microgels are still accessible. Moreover, the catalytic membrane PES/PNM-Ag exhibits higher catalytic performance, indicating that the unique structure of the catalytic membranes further improved the activity. We impute this improvement to the intensification of the mass transfer. It has been reported that the k_{app} value of hybrid microgels utilized for catalytic reduction of 4-NP changes drastically with the swelling/shrinking of the microgel [40]. It is attributed to the variations in the internal diffusion rate of substance, which is strongly connected to the mesh size of the gel network and limits the reaction rate. Whereas, the decisive mechanism of mass transfer in catalytic membranes, forced convection, is more efficient.

In the case of the catalytic membranes fabricated through the in-situ reduction or blending method, all the Ag NPs were located on the pore wall. Pressure encouraged reactants to move through the pores of

Table 1
Comparison of k_{app} and TOF values of the reduction of 4-NP catalyzed by Ag NPs microgels and catalytic membranes.

Catalyst	k_{app} [s^{-1}]	TOF [h^{-1}]	T [°C]	Ref.
PS-NIPA-Ag microgel	1.9×10^{-3}	38.6[a]	20	[40]
PVDF/Ag membrane	0.21[b]	63.3[a]	25	[41]
PVDF/PDA/Ag membrane	0.11[b]	57.7[a]	25	[42]
PES/PNG@Ag membrane	0.12	–	20	[43]
PES/TA-Ag membrane	0.25	–	25	[44]
PES/PNM-Ag membrane	1.12	170.9[a]	20	This work

[a] The TOF here is recalculated by Eqs. (5) and (6).
[b] The k_{app} here is recalculated by Eqs. (2) and (3).

membranes which aided mass transfer and ultimately resulted in an increase in TOF. However, most of the membranes have a pore size of tens to hundreds of nanometers. As a low flux was employed to prolong the residence time, the pores' filtrate was generally considered a laminar flow. Thus the radial mass transfer rate of substance, which was dependent on the diffusion, had a detrimental impact on the overall reaction rate.

The diffusion distance was further shortened by the "3D network" structure in the PES/PNM-Ag membrane. Since swollen microgels deformed to fit and fill in the membrane pores to form a continuous gel network, all Ag NPs in the pores were evenly distributed, with an interparticle distance of a few nanometers. When reactants were brought through the free volume of the gel network by forced convection, the diffusion distance of reactants was equivalent to the thickness of the boundary layer from the bulk fluid to the surface of Ag NPs. The Mears criterion (Eq. (7)) was applied to investigate whether external diffusion limits the reaction.

$$\frac{r_A^{'}\rho_b R_n}{k_c C_{Ab}} < 0.15 \tag{7}$$

where $-r_A^{'}$ is the disappearance rate of species, A per mass of catalyst (mol A g^{-1} s^{-1}), ρ_b is the bulk density of catalyst bed (kg/m^3), R is the radius of catalyst (m), k_c is the mass transfer coefficient (m/s), C_{Ab} is the concentration of A in the bulk fluid. The results of the Mears criterion (10^{-23} << 0.15) manifested that the negative influence of external diffusion on the rate of reaction can be neglected. Furthermore, all the Ag NPs in the gel network were fully exposed instead of covered in the polymer, resulting in increased accessible active sites.

4. Conclusion

In summary, Ag NPs-loaded catalytic membranes with "3D networks" were fabricated by a facile method. It was demonstrated that the catalytic membrane performed superbly and remained stable during continuous operation. The swollen microgels in the pores formed the gel network that acted as both scaffold and a stabilizer for Ag NPs. As a result, they allowed substances to pass through their free volume by forced convection, promoting mass transfer. We believe that these catalytic membranes possess the potential to be developed further for commercial application in green organic synthesis, wastewater treatment and even thin-layer chromatography.

CRediT authorship contribution statement

Yuhua Mao: Investigation, Validation, Writing – original draft. **Hao Zhang:** Supervision, Writing – review & editing. **Saad Ahmed:** Writing – review & editing. **Shanshan Li:** Supervision. **Shouhao Zhang:** Methodology, Investigation. **Jianli Wang:** Conceptualization, Resources, Funding acquisition.

Author contributions

J. Wang conceptualized and administrated the research project. Y. Mao and S. Zhang conducted the experiment and its validation. Y. Mao, H. Zhang and S. Ahmed prepared the manuscript. H. Zhang and S. Li performed the analysis with constructive discussions. All authors reviewed the manuscript.

Declaration of Competing Interest

The authors declare that they have no known competing financial interests or personal relationships that could have appeared to influence the work reported in this paper.

Acknowledgment

This work was sponsored by the National Natural Science Foundation of China (Grants 22178317 and 22109138).

Appendix A. Supplementary material

Supplementary data associated with this article can be found in the online version at doi:10.1016/j.apcatb.2022.121456.

References

[1] J. Vialetto, F. Camerin, F. Grillo, S.N. Ramakrishna, L. Rovigatti, E. Zaccarelli, L. Isa, Effect of internal architecture on the assembly of soft particles at fluid interfaces, ACS Nano 15 (2021) 13105–13117.
[2] G. Chaudhary, A. Ghosh, N.A. Bharadwaj, J.G. Kang, P.V. Braun, K.S. Schweizer, R. H. Ewoldt, Thermoresponsive stiffening with microgel particles in a semiflexible fibrin network, Macromolecules 52 (2019) 3029–3041.
[3] C.C. Cutright, J.L. Harris, S. Ramesh, S.A. Khan, J. Genzer, S. Menegatti, Surface-bound microgels for separation, sensing, and biomedical applications, Adv. Funct. Mater. (2021), 2104164.
[4] B. Jiang, Y. Zhang, X. Huang, T. Kang, S.J. Severtson, W.-J. Wang, P. Liu, Tailoring CO_2-responsive polymers and nanohybrids for green chemistry and processes, Ind. Eng. Chem. Res. 58 (2019) 15088–15108.
[5] F. Li, D. Lyu, S. Liu, W. Guo, DNA hydrogels and microgels for biosensing and biomedical applications, Adv. Mater. 32 (2020), 1806538.
[6] M. Ozawa, Thermal stabilization of catalytic compositions for automobile exhaust treatment through rare earth modification of alumina nanoparticle support, J. Alloy. Compd. 408–412 (2006) 1090–1095.
[7] M.J. Kale, P. Christopher, Utilizing quantitative in situ FTIR spectroscopy to identify well-coordinated Pt atoms as the active site for CO oxidation on Al2O3-supported Pt catalysts, ACS Catal. 6 (2016) 5599–5609.
[8] Y. Chen, M. Wang, L. Zhang, Y. Liu, J. Han, Poly(o-aminothiophenol)-stabilized Pd nanoparticles as efficient heterogenous catalysts for Suzuki cross-coupling reactions, RSC Adv. 7 (2017) 47104–47110.
[9] L.-L. Yang, H.-J. Wang, J. Wang, Y. Li, W. Zhang, T.-B. Lu, A graphdiyne-based carbon material for electroless deposition and stabilization of sub-nanometric Pd catalysts with extremely high catalytic activity, J. Mater. Chem. A 7 (2019) 13142–13148.
[10] S. Fujiwara, N. Takanashi, R. Nishiyabu, Y. Kubo, Boronate microparticle-supported nano-palladium and nano-gold catalysts for chemoselective hydrogenation of cinnamaldehyde in environmentally preferable solvents, Green Chem. 16 (2014) 3230–3236.
[11] F. Liguori, P. Barbaro, Continuous flow synthesis of Rh and Pd nanoparticles onto ion-exchange borate monoliths: application to selective catalytic hydrogenation of unsaturated carbonyl compounds under flow conditions, Catal. Sci. Technol. 4 (2014) 3835–3839.
[12] C. Gao, F. Lyu, Y. Yin, Encapsulated metal nanoparticles for catalysis, Chem. Rev. 121 (2021) 834–881.
[13] L. Shang, J. Xu, G.U. Nienhaus, Recent advances in synthesizing metal nanocluster-based nanocomposites for application in sensing, imaging and catalysis, Nano Today 28 (2019), 100767.
[14] H. Wang, T. Wu, M. Li, Y. Tao, Recent advances in nanomaterials for colorimetric cancer detection, J. Mater. Chem. B 9 (2021) 921–938.
[15] B. Sarkar, P.D. Dissanayake, N.S. Bolan, D.J. Yousuf, M. Kumar, M.N. Haque, R. Mukhopadhyay, S. Ramanayaka, J.K. Biswas, D.C. Tsang, Challenges and opportunities in sustainable management of microplastics and nanoplastics in the environment, Environ. Res. (2021), 112179.
[16] I. Guerrero, A. Saha, J.A.M. Xavier, C. Vinas, I. Romero, F. Teixidor, Noncovalently linked metallacarboranes on functionalized magnetic nanoparticles as highly efficient, robust, and reusable photocatalysts in aqueous medium, ACS Appl. Mater. Interfaces 12 (2020) 56372–56384.
[17] A.P. Ingle, J. Rathod, R. Pandit, S.S. da Silva, M. Rai, Comparative evaluation of free and immobilized cellulase for enzymatic hydrolysis of lignocellulosic biomass for sustainable bioethanol production, Cellulose 24 (2017) 5529–5540.
[18] D. Wang, D. Astruc, Fast-growing field of magnetically recyclable nanocatalysts, Chem. Rev. 114 (2014) 6949–6985.
[19] M. Naz, A. Rafiq, M. Ikram, A. Haider, S.O.A. Ahmad, J. Haider, S. Naz, Elimination of dyes by catalytic reduction in the absence of light: a review, J. Mater. Sci. 56 (2021) 15572–15608.
[20] H. Cheng, Z. Li, Y. Li, Z. Shi, M. Bao, C. Han, Z. Wang, Multi-functional magnetic bacteria as efficient and economical pickering emulsifiers for encapsulation and removal of oil from water, J. Colloid Interface Sci. 560 (2020) 349–358.
[21] S. Wen, Y. Shuang-Ting, W. Yue-Liang, G. Long-Hua, Preparation of noble metal nanoparticles and hydrogel composite materials and their application in analytical chemistry, Chin. J. Anal. Chem. 49 (2021) 676–685.
[22] A. Biffis, N. Orlandi, B. Corain, Microgel-stabilized metal nanoclusters: size control by microgel nanomorphology, Adv. Mater. 15 (2003) 1551–1555.
[23] Y. Tian, S.E. Demirel, M.F. Hasan, E.N. Pistikopoulos, An overview of process systems engineering approaches for process intensification: state of the art, Chem. Eng. Process. 133 (2018) 160–210.

[24] C. Algieri, G. Coppola, D. Mukherjee, M.I. Shammas, V. Calabro, S. Curcio, S. Chakraborty, Catalytic membrane reactors: the industrial applications perspective, Catalysts 11 (2021) 691.
[25] L. Huang, S. Wang, H. Chen, X. Hou, H. Zhang, J. Pan, Y. Zhang, Isolated iron/polyether sulfone catalytic membranes for rapid phenol removal, J. Appl. Polym. Sci. 139 (2022) 51508.
[26] B. Xin, J. Hao, Imidazolium-based ionic liquids grafted on solid surfaces, Chem. Soc. Rev. 43 (2014) 7171–7187.
[27] J. Wang, Z. Wu, T. Li, J. Ye, L. Shen, Z. She, F. Liu, Catalytic PVDF membrane for continuous reduction and separation of p-nitrophenol and methylene blue in emulsified oil solution, Chem. Eng. J. 334 (2018) 579–586.
[28] L. Huang, S. Wang, H. Zhang, D. Li, Y. Zhang, L. Zhao, Q. Xin, H. Ye, H. Li, Enhanced hydrolysis of cellulose by catalytic polyethersulfone membranes with straight-through catalytic channels, Bioresour. Technol. 294 (2019), 122119.
[29] B. Castro-Dominguez, I.P. Mardilovich, L.-C. Ma, R. Ma, A.G. Dixon, N. K. Kazantzis, Y.H. Ma, Integration of methane steam reforming and water gas shift reaction in a Pd/Au/Pd-based catalytic membrane reactor for process intensification, Membranes 6 (2016) 44.
[30] C. De Risi, O. Bortolini, A. Brandolese, G. Di Carmine, D. Ragno, A. Massi, Recent advances in continuous-flow organocatalysis for process intensification, React. Chem. Eng. 5 (2020) 1017–1052.
[31] E. Drioli, A.I. Stankiewicz, F. Macedonio, Membrane engineering in process intensification—an overview, J. Membr. Sci. 380 (2011) 1–8.
[32] R. Begum, J. Najeeb, G. Ahmad, W. Wu, A. Irfan, A.G. Al-Sehemi, Z.H. Farooqi, Synthesis and characterization of poly (N-isopropylmethacrylamide-co-acrylic acid) microgels for in situ fabrication and stabilization of silver nanoparticles for catalytic reduction of o-nitroaniline in aqueous medium, React. Funct. Polym. 132 (2018) 89–97.
[33] D. Menne, F. Pitsch, J.E. Wong, A. Pich, M. Wessling, Temperature-modulated water filtration using microgel-functionalized hollow-fiber membranes, Angew. Chem. Int. Ed. 53 (2014) 5706–5710.
[34] M. Boularas, E. Deniau-Lejeune, V. Alard, J.-F. Tranchant, L. Billon, M. Save, Dual stimuli-responsive oligo (ethylene glycol)-based microgels: insight into the role of internal structure in volume phase transitions and loading of magnetic nanoparticles to design stable thermoresponsive hybrid microgels, Polym. Chem. 7 (2016) 350–363.
[35] N.R. Richbourg, N.A. Peppas, The swollen polymer network hypothesis: quantitative models of hydrogel swelling, stiffness, and solute transport, Prog. Polym. Sci. 105 (2020).
[36] Q. Zhang, Z. Wang, L. Lei, J. Tang, J. Wang, S. Zhu, CO_2-switchable membranes prepared by immobilization of CO_2-breathing microgels, ACS Appl. Mater. Interfaces 9 (2017) 44146–44151.
[37] M.I. Din, R. Khalid, Z. Hussain, T. Hussain, A. Mujahid, J. Najeeb, F. Izhar, Nanocatalytic assemblies for catalytic reduction of nitrophenols: a critical review, Crit. Rev. Anal. Chem. 50 (2020) 322–338.
[38] T. Kanti Das, S. Ganguly, S. Remanan, N.C. Das, Temperature-dependent study of catalytic Ag nanoparticles entrapped resin nanocomposite towards reduction of 4–nitrophenol, ChemistrySelect 4 (2019) 3665–3671.
[39] G.H. Choi, K. Rhee do, A.R. Park, M.J. Oh, S. Hong, J.J. Richardson, J. Guo, F. Caruso, P.J. Yoo, Ag nanoparticle/polydopamine-coated inverse opals as highly efficient catalytic membranes, ACS Appl. Mater. Interfaces 8 (2016) 3250–3257.
[40] Y. Lu, Y. Mei, M. Drechsler, M. Ballauff, Thermosensitive core–shell particles as carriers for Ag nanoparticles: modulating the catalytic activity by a phase transition in networks, Angew. Chem. Int. Ed. 45 (2006) 813–816.
[41] X. Chen, Z. Wang, S. Bi, K. Li, R. Du, C. Wu, L. Chen, Combining catalysis and separation on a PVDF/Ag composite membrane allows timely separation of products during reaction process, Chem. Eng. J. 295 (2016) 518–529.
[42] S. Ma, X. Chen, B. Zhao, H. Dong, Q. Yuan, L. Li, J. Lv, L. Shi, L. Chen, Facile preparation of a silver nanoparticles-containing membrane with an enhanced catalysis and separation, Appl. Catal. A 536 (2017) 35–44.
[43] R. Xie, F. Luo, L. Zhang, S.F. Guo, Z. Liu, X.J. Ju, W. Wang, L.Y. Chu, A. Novel, Thermoresponsive catalytic membrane with multiscale pores prepared via vapor-induced phase separation, Small 14 (2018), e1703650.
[44] X. Fang, J. Li, B. Ren, Y. Huang, D. Wang, Z. Liao, Q. Li, L. Wang, D.D. Dionysiou, Polymeric ultrafiltration membrane with in situ formed nano-silver within the inner pores for simultaneous separation and catalysis, J. Membr. Sci. 579 (2019) 190–198.
[45] A.J. Plomp, H. Vuori, A.O.I. Krause, K.P. de Jong, J.H. Bitter, Particle size effects for carbon nanofiber supported platinum and ruthenium catalysts for the selective hydrogenation of cinnamaldehyde, Appl. Catal. A 351 (2008) 9–15.